Finite Element Methods for Multi-objective optimization of a High Step-up Interleaved Boost Converter

Martinez, Wilmar; Cortes, Camilo A.; Ahmad, Bilal; Kyyrä, Jorma

Finite Element Methods for Multi-objective optimization of a High Step-up Interleaved Boost Converter

Published in:
Proceedings of the International Power Electronics Conference, IPEC-Niigata - ECCE Asia 2018

DOI:
10.23919/IPEC.2018.8507786

Published: 01/01/2018

Document Version
Peer reviewed version

Please cite the original version:
Martinez, W., Cortes, C. A., Ahmad, B., & Kyyrä, J. (2018). Finite Element Methods for Multi-objective optimization of a High Step-up Interleaved Boost Converter. In Proceedings of the International Power Electronics Conference, IPEC-Niigata - ECCE Asia 2018 (pp. 2193-2198). Institute of Electrical and Electronics Engineers. https://doi.org/10.23919/IPEC.2018.8507786

Finite Element Methods for Multi-objective optimization of a High Step-up Interleaved Boost Converter

Wilmar Martinez[1,2*], Camilo Cortes[2], Ahmad Bilal[3], and Jorma Kyyra[3]
[1] KU Leuven, Campus Diepenbeek, Belgium
[2] Universidad Nacional de Colombia, Bogota, Colombia
[3] Aalto University, Espoo, Finland
*E-mail: wilmar.martinez@kuleuven.be

Abstract— **High step-up converters have been widely used in renewable energy systems and, recently, in automotive applications, due to their high voltage gain capability. In these applications, efficiency and high-power density are usually required, although these characteristics are commonly opposite objectives. Therefore, a multi-objective optimization is quite useful in order to comply with both requirements of high efficiency and small size. In that sense, the Finite Element Method can be effective to complement optimization methods. This paper presents a procedure to optimize the efficiency and the volume of a high step-up converter that utilizes a coupled inductor with three windings installed in only one core. This optimization procedure is carried out using 3D and 2D Finite Element Method simulations. In this procedure, a complete modeling of power losses, size, and flux density is evaluated by comparing different materials and dimensions. The results of this modeling stage are introduced into a multi-objective optimization algorithm to obtain a Pareto front. Finally, the optimization methodology is validated by experimental tests.**

Keywords— Finite Element Methods, High Step-Up Converter, Efficiency, Power Density.

I. INTRODUCTION

High Step-Up (HSU) converters are able to boost low voltages to obtain much higher voltages required by the application load. Usually, HSU converters are used in systems where the power source has low voltage storage cells that need to power industrial applications such as Uninterruptible Power Systems, communication systems, renewable energy appliances, grid-connected systems, electric mobility, among others [1]-[7].

These converters become useful due to their advantages of high voltage gain, which is quite higher in comparison with the conventional and the interleaved boost topologies. Conventional topologies require an extremely high duty cycle to achieve the required gain, and high duty cycles generate large losses. Moreover, parasitic components play an important role in HSU converters because they hamper the conventional voltage-gain at high duty cycles. When a large duty cycle is in operation, the voltage-gain tends to decrease because of the parasitic components [7]-[9].

Nevertheless, most of the HSU converters evidence limitations of efficiency and power density because of the complex circuitry with abundant components that increase its size. These additional components may be bulky and heavy, increase the volume and mass of the circuit and compromise the converter power density and, in many cases, the efficiency as well [10]-[12].

Consequently, multi-objective optimization of efficiency and power density of these converters is needed to obtain suitable designs for the applications mentioned above. These optimization procedures are required in applications where power density and efficiency are critical, like electric mobility or renewable energies [13]-[19].

This study analyses an HSU converter with a novel coupled-inductor capable of increasing the power density and the voltage gain. This converter acquires an outstanding performance thanks to the combination of the techniques of magnetic coupling and interleaving phases, which are effective for downsizing inductive and capacitive components in DC-DC converters [20]-[22]. Also, from the physics point of view, a reduction in the magnetic core size could represent a direct reduction on the iron losses [23]. Consequently, this HSU converter offers an outstanding high voltage gain without the addition of many semiconductors or bulky inductors and capacitors.

In addition, an optimization procedure is implemented to design an HSU converter suitable for applications where high-power density and efficiency are required. In this procedure, 3D and 2D Finite Element Method (FEM) simulations are conducted in COMSOL to complement the analytical models, and estimate the power losses in the magnetic core and shielding materials, the magnetic stray fields, and the temperature rise in the materials.

This paper is organized in four sections. First, the review of the operating principle of the analyzed converter is presented. The ideal and non-ideal voltage gain is reviewed as well. Second, the optimization

procedure is presented; the power loss analysis and the FEM simulations are conducted. Then, the Pareto front is obtained from the optimization procedure and from the 3D FEM simulations. Finally, a 1kW prototype, built for the validation of the theoretical analysis, is experimentally tested.

II. Review Of The High Step-Up Converter

A. Circuit Configuration

The analyzed HSU converter, shown in Fig. 1, is a two-phase interleaved boost converter composed of a magnetic coupled-inductor with three windings that are installed in only one magnetic core. This core can be constructed with different three-leg shapes (usually EE, EI, EER, EC cores). Two windings, L_1 and L_2, are connected to the power source and a central winding L_c (usually installed in the center of the three-leg core) is located between the anodes of D_3 and D_4. For convenience, the positive terminal of Lc is defined as the node where the cathode of D_1 and the anode of D_3 are connected. In addition, this HSU converter has two power switches, S_1 and S_2, which are alternatively commuted with a phase difference of 180-degrees between them. Finally, the converter is composed of four diodes D_1-D_4, and one output capacitor C_o, as well.

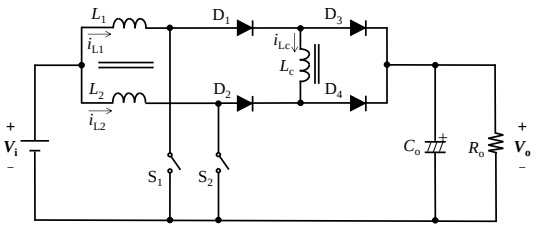

Fig. 1. High step-up converter with coupled inductor.

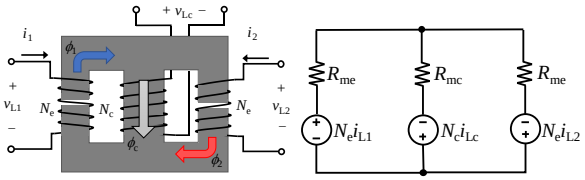

(a) Flux flow (b) Magnetic Model

Fig. 2. Coupled-inductor with 3 windings.

Fig. 2 depicts the representation of the coupled-inductor shown in Fig. 1 using an EE core. The magnetic component of this converter has three windings that share the same core. The outer windings are directly coupled. An air-gap is placed in each outer leg to suppress DC flux induction. Three different magnetic fluxes are circulating through the core (Fig. 2(a)) and three magnetic reluctances can be defined (Fig. 2(b)). ϕ_1, ϕ_2 and ϕ_c are the external and central magnetic fluxes in the EE core; *Ne* and *Nc* are the number of turns of the external windings and the central one, respectively; R_{me} and R_{mc} are the magnetic reluctances of the external and central legs, respectively; and i_{L1}, i_{L2}, and i_{LC} are the currents flowing through each winding.

B. Operating Principle

Fig. 3 shows the operating waveforms of the converter under an ideal and a continuous conduction operation. Fig. 3a shows the case when the duty cycle *d* is lower than 50%, and Fig. 3b when it is higher than 50%. As it is well known, when a converter has an interleaved two-phase operation, it has at least two duty cycle cases with different performances.

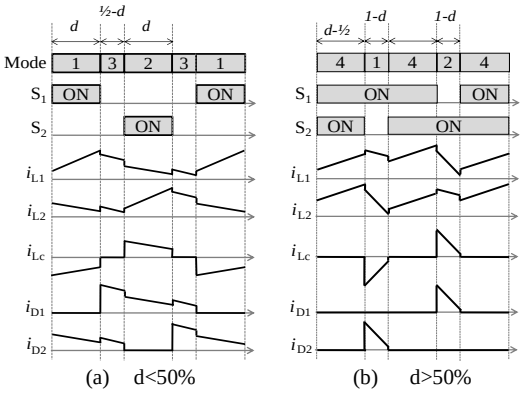

(a) d<50% (b) d>50%

Fig. 3. Duty cycle cases.

As many other two-phase interleaved converters, the analyzed converter presents four operating modes. Each operating mode is shown in Fig. 4. Modes 1, 2 and 3 correspond to the case of duty cycles d<0.5, and Modes 1, 2 and 4 are presented in the case d>0.5. The complete description of each operating mode and the steady-state analysis are presented in [22].

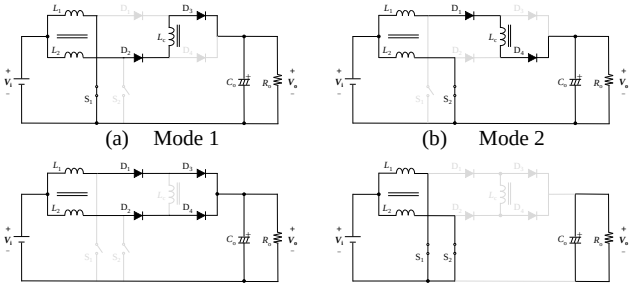

(a) Mode 1 (b) Mode 2

(c) Mode 3 (d) Mode 4

Fig. 4. Operating modes.

To put in context the effectiveness of this converter, its voltage gain is reviewed. Considering the analysis of [22] and the definition of *N* as the ratio between the number of turns of the central leg and the external legs (*N=Nc/Ne*), the voltage gain *M* of both duty cycle cases is derived as follows:

$$M_{d<0.5} = \frac{V_o}{V_i} = \frac{1+N}{(1+N)-d(1+2N)} \quad (1)$$

$$M_{d>0.5} = \frac{V_o}{V_i} = \frac{1+N}{1-d} \quad (2)$$

where V_o and V_i are the output and input voltages.

Fig. 5 shows the ideal voltage gain with different turn

ratios, based on (1) and (2).

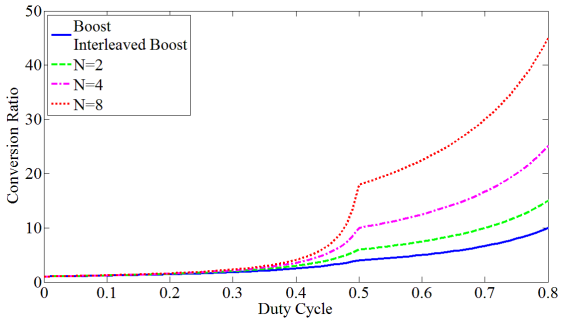

Fig. 5. Ideal conversion ratio.

Nevertheless, as it was mentioned above, parasitic components are important in HSU converters. The non-ideal voltage gain can be calculated as shown in Fig. 6. Fig. 6 considers different cases of ratios between the parasitic resistances R_L and the load R_o and proves the importance of parasitic components in HSU converters. It is possible to conclude that when the ratio between the parasitic resistances in the windings and the resistance of the load increases, the voltage gain is increasingly affected [20].

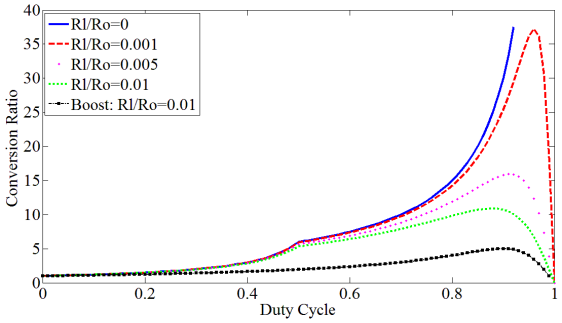

Fig. 6. Non-Ideal conversion ratio vs. Duty cycle.

III. Optimization Procedure

The first analysis of the optimization procedure is the power loss analysis. Then, several constraints and objective functions are defined. In the case of the converter efficiency, it is optimum when the following objective function is minimized:

$$\min \begin{bmatrix} P_{Loss} = P_{Lcore}(f_{sw}, k_{core}) + P_{Lcopper}(f_{sw}, k_w) + \\ P_C(f_{sw}, k_C) + P_{TR}(f_{sw}, k_{TR}) + P_D(f_{sw}, k_D) \end{bmatrix} \quad (3)$$

where each k corresponds to the particular factors of each component needed to calculate their individual power losses. In addition, f_{sw} is the switching frequency and it is one of the main variables that affect the optimization procedure. As it is well-known, increasing the switching frequency (until certain values) can be beneficial for reducing the converter size but harmful for the power conversion efficiency.

Moreover, in order to calculate and minimize the power losses and the converter size, an analytical algorithm is conducted. This analytical calculation is carried out following the steps of the design procedure presented in Fig. 7.

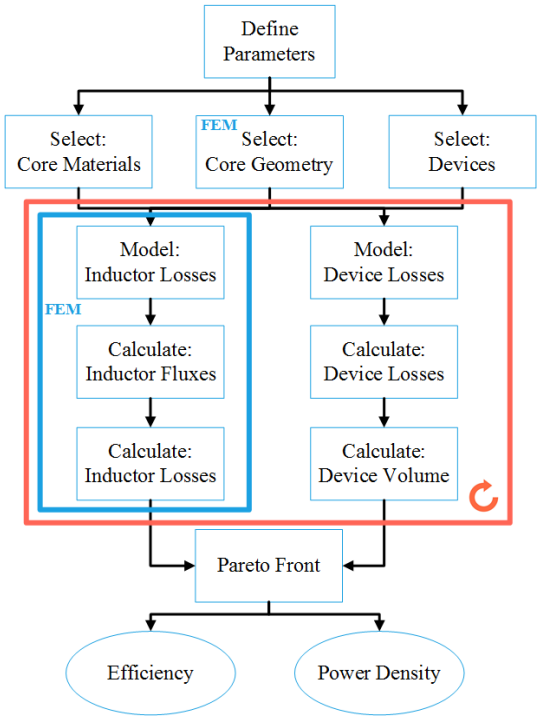

Fig. 7. Design procedure.

In the design procedure of Fig. 7, it is highlighted that part of the optimization is conducted using FEM simulations. The coupled-inductor is simulated with the evaluation of magnetic and electrical fields through time dependent and frequency domain studies.

Taking as a case study of this particular procedure, the parameters presented in Table I were chosen to validate the effectiveness of the proposed methodology.

TABLE I
Circuit Parameters

Input Voltage V_i [V]	80
Output Voltage V_o [V]	200
Turn Ratio N	2
Power P [kW]	1
Switching Frequency f_{sw} [kHz]	15-200

In this procedure, several soft-magnetic materials were considered. In addition, silicon, silicon carbide, and gallium nitride semiconductors were selected for this optimization study, as well as film, electrolytic, and multi-layer ceramic capacitors. All these components are evaluated in the procedure of Fig. 7, considering different switching frequencies, number of turns, possible core geometries, and coupling factors. Table II shows a review of the characteristics of the magnetic materials selected for this case study. Table III and Table IV show the characteristics of the Mosfets and Diodes selected for this study, respectively. In total, 70 Mosfets, 70 Diodes, and 30 magnetic materials were considered in this case study. Diodes and Mosfets were selected at ratings of 650V and average 20A.

TABLE II
MAGNETIC MATERIAL CHARACTERISTICS

Material	Relative Permeability	Losses [mW/cm^3]*	Saturation Flux [T]**
Micrometals Powdered Iron	35~75	600~1300	~0.5
Magnetics Kool M	60~125	~200	~1
Magnetics Molypermalloy	60~550	87~890	~0.8
Magnetics High Flux	14~160	290~1280	~1.5
Magnetics Ferrite	2000~3000	5~38	0.45~0.47
TDK Ferrite	2000~2500	14~21	~0.35
FairRite	~1500	~85	~0.5

*Loss at 100kHz 50 mT **Remanent flux excluded

TABLE III
MOSFET CHARACTERISTICS

Manufacturer	Ciss [nF]	Coss [pF]	Ron [mΩ]
STM	0.78~9.6	~300	45~299
Fairchild	1~1.415	~35	165~250
Infineon	0.95~1.5	~750	26~280
ROHM SiC	~0.852	~55	60~196
Panasonic GaN	~0.405	~71	70~290
On Semi GaN	~0.760	~26	340~350
GaN Systems	~0.520	~130	25~560
Transphorm GaN	0.72~1.13	~56	72~180

TABLE IV
DIODE CHARACTERISTICS

Manufacturer	trr [ns]	Qr [nF]	Vd [V]
Fairchild	50~80	0.29~65	0.7~1.5
ROHM SiC	0~60	0.21~0.73	1.05~1.55
CREE SiC	~	0.29~1.1	1.45~1.8
Infineon SiC	0 ~13.7	0.19~1.14	1.35~1.7

IV. FEM PROCEDURE

A. Optimization Solvers using FEM

As Fig. 7 shows, FEM procedures were conducted for two main purposes. The first one was the core geometry optimization using a 2D FEM simulation and applying a topology optimization procedure for the case of an EE core.

The second FEM procedure was used for the calculation and modeling of magnetic fluxes and core losses. In this case, a 3D FEM simulation was conducted based on the results of the 2D procedure.

As it is well-known, different optimization procedures can be conducted in FEM software. As an example, COMSOL offers different optimization modules capable of solving different problems with both Gradient-Free and Gradient-Based methods. In these modules, several methods can be implemented, *inter alia*, Random, 1st and 2nd order approximate gradient, Linear, quadratic [24].

B. 2D FEM Simulation

As it was mentioned above, a 2D FEM simulation was conducted in order to implement a topology optimization algorithm. In this context, the main dimensions of a three- leg EE core (see Fig. 2) were evaluated in this algorithm using the parameters of the case study presented in Table I.

Fig. 8 shows the case of the core EC70 PC40 manufactured by TDK driven at a frequency of 200kHz. Fig. 8a shows that the evaluated core is oversized because it has an average magnetic flux of nearly 150mT when its saturation flux is 250mT (having in mind the remanent flux). In addition, Fig. 8b shows the arrow surface magnetic flux, where it is possible to see the effect of the direct coupling between the external windings.

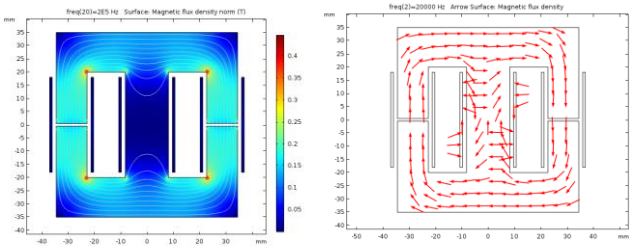

(a) Surface [T] (b) Arrow Surface

Fig. 8. Magnetic Flux Density in the EE core.

As a result of this topology optimization procedure, the core EE50 PC40 was selected for the case study described above. This core is much smaller than the one that was originally selected and that have been tested in previous studies [20][22].

C. 3D FEM Simulation

A 3D FEM simulation was conducted in order to calculate the magnetic fluxes and the power losses in the evaluated cores. At the same time, these simulations served as a validation of the coupled-inductor operation. This validation was possible via the verification of the lack of saturation in the core.

Fig. 9 shows the 3D FEM component of the originally selected core (EC70). This component was modeled with a mesh of 300 thousand elements with sizes between 15 and 3 mm.

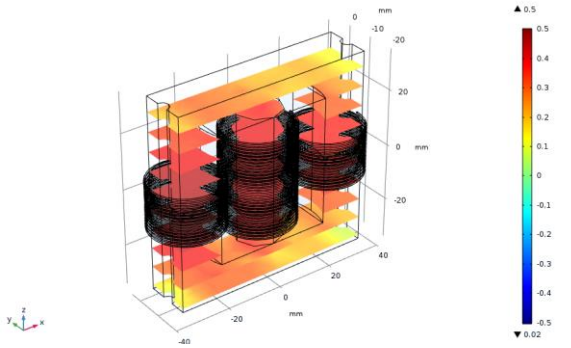

Fig. 9. FEM Model of the HSU Coupled-Inductor.

After the 3D FEM simulations, the loss evaluation and power density of transistors, diodes, and capacitors of the HSU converter are considered in order to find the suitable operating conditions that offer the lowest power losses and the highest power density.

V. Converter Test Results

Taking into account the components of Table II-IV, the parameters of Table I, and the optimization method using FEM described above, the full design procedure of Fig. 7 was conducted.

As a result, the Pareto-Front of Fig. 10 was obtained. Fig. 10 shows many points that correspond to all the possible designs of the coupled inductor at different conditions in the selected HSU converter. In this figure, efficiencies higher than 90% and their possible power densities are presented. As a matter of fact, it is important to notice that the efficiency and power density values correspond to the case of the inductor only, without considering cooling and casing systems.

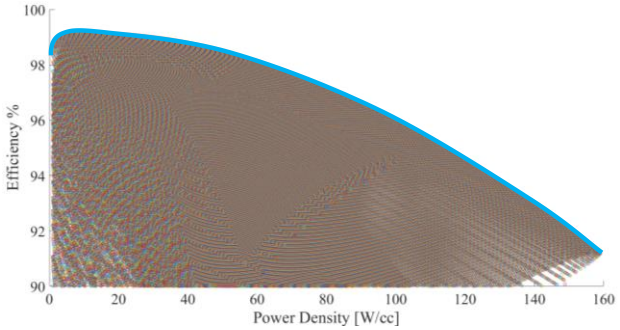

Fig. 10.Efficiency – Power Density Pareto representation of the coupled inductor.

The next step, after having the pareto front, is the selection of one points of the pareto front. In that case, many aspects can affect the selection process: cost, component availability, special requirements on size and/or efficiency, etc. Therefore, a decision-making procedure can be effective for the selection of the suitable point. In the case of this evaluation, the procedure of the 2D simulation and the component availability influenced the decision.

To validate the optimization procedure presented in the previous sections, an experimental validation was conducted. Therefore, two 1kW-prototypes were constructed with a core EE50, SiC Diodes, and one Multilayer Ceramic Capacitor. One prototype was constructed with SiC Mosfets and the other with GaNFETs. These circuits were tested using the parameters of Table I. The efficiency tests were measured with a Precision Power Analyzer. Fig. 11 shows the prototype of the HSU converter with GaNFETs.

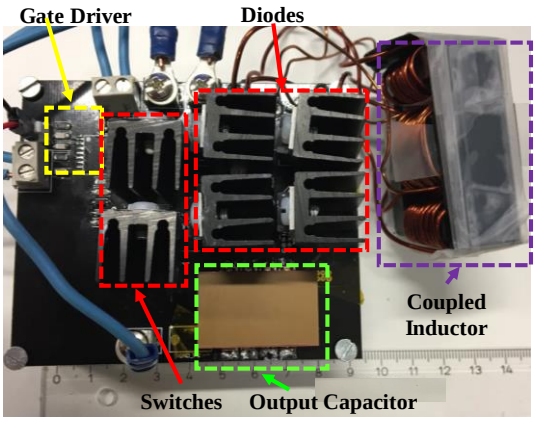

Fig. 11.Prototype of the HSU converter with GaNFETs.

Efficiency and volume measurements were conducted. The 1kW prototypes were tested at the conditions that the Pareto front provided. In these measurements, additional parasitic components such as the ESR of the output capacitor and the ESR of the terminals were neglected in the optimization procedure. Therefore, it is planned to take them into account in future optimization procedures.

Four switching frequencies were tested for the case of both converters. Fig. 12-15 show the efficiency and the voltage gain measured during the experimental tests.

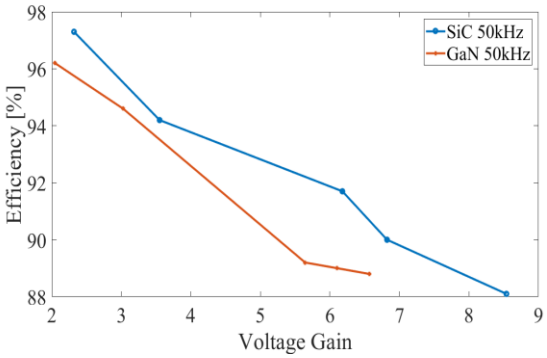

Fig. 12.Efficiency vs. Voltage Gain at 50kHz.

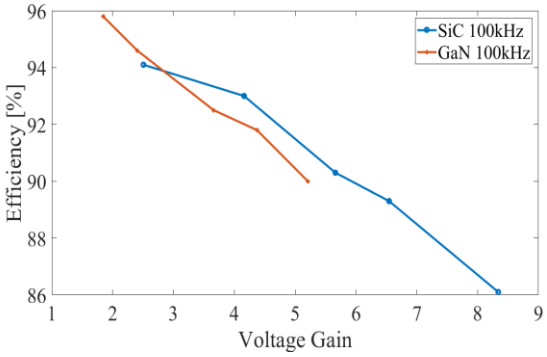

Fig. 13.Efficiency vs. Voltage Gain at 100kHz.

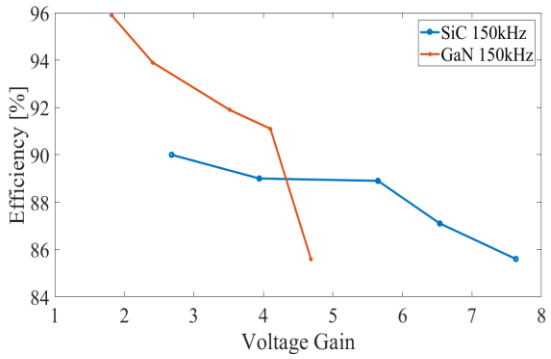

Fig. 14.Efficiency vs. Voltage Gain at 150kHz.

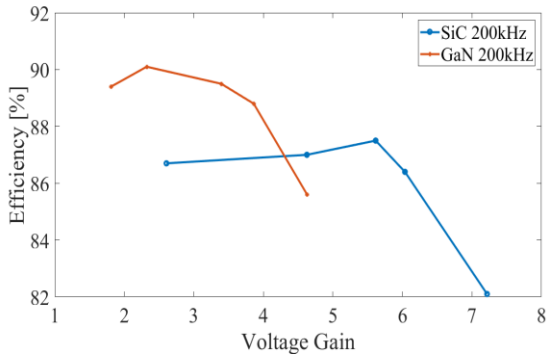

Fig. 15.Efficiency vs. Voltage Gain at 200kHz.

It is possible to notice that the voltage gain that the GaNFETs presented was lower than the one of the SiC Mosfets. This behavior was observed due to the parasitic conditions of the GaN switches. On the other hand, at frequencies higher than 100kHz, GaN switches presented higher efficiency than the prototypes with SiC switches.

It is important to mention that using multi-objective optimization procedures always leads to different solutions that must be considered with the use of constrains and limitations. In the case of applications where high voltage gain is required, the use of SiC would be suitable considering the selected case study.

Finally, the constructed prototype showed a power density around 2.5W/cc, without casing and cooling systems (despite the heatsinks).

VI. Conclusions

An optimization methodology that combines analytical calculation of power losses and power density with 2D and 3D FEM simulations of the coupled inductor in a novel HSU converter is presented and evaluated in this paper. This optimization procedure takes into account emerging technologies of semiconductors, novel magnetic materials, different core geometries and sizes, as well as several design conditions like number of turns, magnetic coupling, and switching frequency. This methodology was conducted with an analytical calculation of an optimization algorithm where FEM simulations were integrated. As a result, the efficiency – power density Pareto front was obtained. It was found that this procedure is effective to select the suitable core size for a converter with specific parameters.

References

[1] L. Schmitz et al, "Design optimization of a high step-up DC-DC converter for photovoltaic microinverters," *2017 IEEE International Telecommunications Energy Conference (INTELEC)*, pp. 432-437, 2017.

[2] T. S. Lakshmi and P. R. Rao, "High voltage gain boost converter for micro grid application," *2012 Annual IEEE India Conference (INDICON)*, pp. 323-328, 2012.

[3] G. Cao et al, "A high step-up modular DC/DC converter for photovoltaic generation integrated into DC grids," *43rd Annual Conference of the IEEE Industrial Electronics Society*, pp. 4421-4426, 2017.

[4] W. Martinez, C. Cortes, M. Yamamoto, J. Imaoka and K. Umetani, "Total Volume Evaluation of High Power Density Non-Isolated DC-DC Converters with Integrated Magnetics for Electric Vehicles," *IET Power Electronics*, vol.10, no.14, pp. 1755-4535, Nov. 2017.

[5] G. Wu, X. Ruan and Z. Ye, "High Step-Up DC-DC Converter Based on Switched Capacitor and Coupled Inductor," *IEEE Transactions on Industrial Electronics*, vol. 65, no.7, pp. 5572-5579, 2018.

[6] H. C. Liu and F. Li, "Novel High Step-Up DC–DC Converter with an Active Coupled-Inductor Network for a Sustainable Energy System," *IEEE Transactions on Power Electronics*, vol. 30, no.12, pp. 6476-6482, 2015.

[7] C.-T. Pan, C.-F. Chuang, and C.-C. Chu, "A Novel Transformer-less Adaptable Voltage Quadrupler DC Converter with Low Switch Voltage Stress," *IEEE Trans. Power Electron*., vol. 29, no. 9, pp. 4787–4796, Sep. 2014.

[8] Z. Zhang, and L. Zhou, "Analysis and design of isolated flyback voltage-multiplier converter for low-voltage input and high-voltage output applications," *IET Power Electron*., vol. 6, no. 6, pp. 1100–1110, 2013.

[9] K.-C. Tseng, C.-C. Huang, and C.-A. Cheng, "A Single-Switch Converter with High Step-Up Gain and Low Diode Voltage Stress Suitable for Green Power-Source Conversion," *IEEE J. Emerg. Sel. Top. Power Electron*., vol. 4, no. 2, pp. 363–372, Jun. 2016.

[10] W. Martinez, J. Imaoka, Y, Itoh, M. Yamamoto and K. Umetani "A Novel High Step-Down Interleaved Converter with Coupled Inductor," *IEEE International Telecommunications Energy Conference - INTELEC*, pp. 1-6, Oct, 2015.

[11] M. Pavlovsky, G. Guidi, and A. Kawamura, "Assessment of Coupled and Independent Phase Designs of Interleaved Multiphase Buck/Boost DC-DC Converter for EV Power Train," *IEEE Trans. Power Electron*., vol. 29, no. 6, pp. 2693–2704, 2014.

[12] K. Park, G. Moon, and M. Youn, "Non-isolated high step-up stacked converter based on boost-integrated isolated converter," *IEEE Trans. Power Electron*., vol. 26, no. 2, pp. 577–587, 2011.

[13] J. M. Myrzik and M. Calais, "String and module integrated inverters for single-phase grid connected photovoltaic systems-a review," *Power Tech Conference*, pp. 1-8, 2003.

[14] D. Pal, H. Koniki and P. Bajpai, "Central and micro inverters for solar photovoltaic integration in AC grid," *National Power Systems Conference (NPSC)*, pp. 1-6, 2016.

[15] S. B. Kjaer, J. K. Pedersen and F. Blaabjerg, "Power inverter topologies for photovoltaic modules-a review," *37th IAS Annual Meeting. Conference*, pp. 782-788, 2002.

[16] S. B. Kjaer, J. K. Pedersen and F. Blaabjerg, "A review of single-phase grid-connected inverters for photovoltaic modules," *IEEE Trans. Ind. Appl*., vol. 41, no.5, pp. 1292-1306, 2005.

[17] B. Xiao et al, "Modular cascaded H-bridge multilevel PV inverter with distributed MPPT for grid-connected applications," *IEEE Trans. Ind. Appl*., vol. 51, no.2, pp. 1722-1731, 2015.

[18] M. Hirakawa et al., "High power density interleaved DC/DC converter using a 3-phase integrated close-coupled inductor set aimed for electric vehicles," in 2010 *IEEE Energy Conversion Congress and Exposition*, pp. 2451–2457, 2010.

[19] B. Ahmad, W. Martinez, and J. Kyyra, "Efficiency Optimization of Interleaved High Step-Up Converter," *9th International Conference on Power Electronics, Machines and Drives - PEMD*, pp. 1-6, Apr, 2018.

[20] W. Martinez, C. Cortes, J. Imaoka and M. Yamamoto, "Parasitic Resistance Effect on the Voltage-Gain of High Step-Up DC-DC

Converters for Electric Vehicle Applications," *IET Power Electronics*, vol.PP, no.99, (11 Pages), Jan. 2018
[21] W. Josias de Paula, D. de S. Oliveira Júnior, D. de C. Pereira, and F. L. Tofoli, "Survey on non-isolated high-voltage step-up dc–dc topologies based on the boost converter," IET Power Electron., vol. 8, no. 10, pp. 2044–2057, Oct. 2015.
[22] W. Martinez, J. Imaoka, M. Yamamoto, and K. Umetani, "High Step-Up Interleaved Converter for Renewable Energy and Automotive Applications," in 4th International Conference on Renewable Energy Research and Applications, pp. 1–6. 2015.
[23] W. Martinez, S. Odawara, and K. Fujisaki, "Iron Loss Characteristics Evaluation Using a High Frequency GaN Inverter Excitation," *IEEE Transactions on Magnetics*, vol. 53, no. 11, pp. 1-7, Jun. 2017.
[24] W. Frei, "Optimization with COMSOL Multiphysics," COMSOL Tokyo Conference 2014, pp. 1-55, 2014.